Dispersive properties of finite, one-dimensional photonic band gap structures: Applications to nonlinear quadratic interactions

M. Centini,[1] C. Sibilia,[1,*] M. Scalora,[2,3,†] G. D'Aguanno,[1,2] M. Bertolotti,[1] M. J. Bloemer,[2] C. M. Bowden,[2] and I. Nefedov[4]

[1]*INFM at Dipartimento di Energetica, Università di Roma ''La Sapienza,'' Via Scarpa 16, 00161 Roma, Italy*

[2]*U.S. Army Aviation and Missile Command, Weapon Sciences Directorate, AMSMI-RD-WS-ST Redstone Arsenal, Huntsville, Alabama 35898-5000*

[3]*Time Domain Corporation, 6400 Odyssey Drive, Huntsville, Alabama 35898*

[4]*Institute of Radio Engineering and Electronics, Academy of Sciences, Saratov Branch, Zelyonaya Street 38, Saratov 410019, Russia*

(Received 21 May 1999)

We discuss the linear dispersive properties of finite one-dimensional photonic band-gap structures. We introduce the concept of a complex effective index for structures of finite length, derived from a generalized dispersion equation that identically satisfies the Kramers-Kronig relations. We then address the conditions necessary for optimal, phase-matched, resonant second harmonic generation. The combination of enhanced density of modes, field localization, and exact phase matching near the band edge conspire to yield conversion efficiencies orders of magnitude higher than quasi-phase-matched structures of similar lengths. We also discuss an unusual and interesting effect: counterpropagating waves can simultaneously travel with different phase velocities, pointing to the existence of two dispersion relations for structures of finite length.
[S1063-651X(99)15010-4]

PACS number(s): 42.70.Qs, 42.65.Ky

I. INTRODUCTION

Recently, one-, two-, and three-dimensional periodic structures [1–3] have attracted a great deal of attention in the optics community because these structure may hold the key to significant technical advances in the field. The essential property of these structures, often referred to as photonic band-gap (or PBG) structures, is the existence of allowed and forbidden frequency bands and gaps, in analogy to the allowed and forbidden energy bands and gaps of semiconductors.

The simplest types of PBGs are one-dimensional (1D), periodic or quasiperiodic multilayer stacks, which will be the focus of our discussion. By way of a brief review, we note that significant potential applications for a broad class of 1D linear and nonlinear optical devices have recently been proposed. The list of applications include a nonlinear optical limiter [4] and a diode [5], photonic band-edge laser [6], true-time delay line [7], a high-gain optical parametric amplifier for nonlinear frequency conversion [8], and, more recently, transparent metal-dielectric stacks [9]. Here, we will not discuss 2D and 3D structures, but point out that, for example, in two dimensions, photonic crystal fibers (PCFs) were recently developed [10]. In our view, PCFs represent the most significant advance in guided-wave structures in recent memory because of their unique properties. In 3D, PBG applications in the optical regime still remain elusive due to the difficulties associated with the fabrication or growth of structures with lattice constants only a few hundreds of nanometers in length. However, some demonstrations of the potential of these structures have been made in the microwave regime with the recent development of a PBG metal substrate for applications to antenna structures [11].

In this paper, we first discuss the *general* linear dispersive properties that characterize finite 1D structures, and then study how they affect resonant nonlinear quadratic interactions of the type first discussed in Ref. [8]. Growing interest in second-harmonic generation (SHG) is reflected by the large number of recent publications on this topic (see Ref. [8] and references therein). The importance of parametric interactions such as SH generation, and frequency up- and down-conversion in general, is due to the unavailability of laser radiation at frequencies that are not accessible through more direct processes. SH generation and its enhancement in periodic structures was first proposed in Ref. [12]. Introducing a periodic modulation in the refractive index, phase-matching conditions for SH generation may be satisfied. Various phase-matching schemes have been proposed, such as using uniform Bragg grating [13], local defect modes within the forbidden band [14–16], and introducing corrugations in thin-film waveguides [17]. These cavity-enhancement schemes are based on the use of resonant peaks for either the pump or the SH field. To our knowledge, optimal conditions for nonlinear interactions have never been discussed for structures having a *small* number of periods with *large index discontinuities*, where it is possible to (a) resolve individual transmission resonances; (b) have a high density of modes near the band edge; and, as we will show below, (c) achieve exact phase matching.

Our present work is motivated mainly by the results discussed in Ref. [8]. In that work, it was numerically established that SH generation near the band edge of a finite PBG structure with deep gratings may be enhanced by several orders of magnitude compared to SH generation from a phased-matched bulk sample of similar length. A scheme for doubly resonant second harmonic generation near the band

*FAX: +39 06 442 40183.
Electronic address: sibilia@axrma.uniromal.it
†Electronic address: mscalora@ws.redstone.army.mil

edge of a finite, 1D PBG structure was proposed. The pump and the second harmonic fields are tuned at transmission resonances near their respective band edges, where the density of modes is high, group velocity is low, field localization and overlap are strong, and, consequently, interaction times are longer. The idea of using band-edge resonances to enhance nonlinear processes results primarily from an interesting effect relating to linear pulse propagation: short, picosecond pulses can propagate at speeds much less than *c*, the speed of light in vacuum, with minimal distortion and scattering losses through the structure [7]. These results strongly suggested at the time that while phase-matching conditions were important, *and not well understood*, a high density of modes was necessary in order to enhance conversion efficiencies well above the values obtained from phase-matched bulk media. That is, the combination of high mode density and phase matching creates the conditions that are necessary to observe the unusually large conversion efficiencies theoretically demonstrated for the first time in Ref. [8].

We therefore set out to understand the phase properties of finite multilayer stacks, and for this purpose we introduce the concept of ''complex effective index'' for a structure of finite length. The concept of effective index is not new [12,17,18]. However, we can summarize the innovations in our approach as follows. First, we solve Maxwell's equations by applying boundary conditions in the presence of entry and exit interfaces, i.e., all the variables introduced take into account the fact that the structure has finite length. Second, the method presented is general, and not necessarily restricted to periodic structures. Third, we demonstrate that the complex effective index derived in this way identically satisfies the Kramers-Kronig relations, and hence it is causal. Fourth, we emphasize the importance of the density of modes in the calculation of the conversion efficiency in nonlinear interactions. To our knowledge, the density of modes has never been explicitly invoked simultaneously with phase matching conditions, and we note that the complex effective index that we introduce is completely determined by the linear properties of the structure. Although nonlinear index shifts are always present in the dynamics, typically they remains three to four orders of magnitude smaller compared to the linear index modulation of the structure, which, as in Ref. [8], is of order unity. The model can be modified to include band-edge shifts in the case of fiber Bragg gratings, for example, but that is beyond the scope of the current analysis. Finally, we will also briefly mention an interesting related effect also never noted before, to our knowledge. For a structure of finite length, we show by direct integration of the equations of motion that counterpropagating waves can travel with different instantaneous phase velocities, pointing to the existence of two dispersion relations, in part predicted by our effective index model.

II. DISPERSION RELATION FOR FINITE PBG

We consider 1D, linear PBG materials. We seek an explicit dispersion relation for a structure of finite length, and we begin by writing the complex transmission coefficient for the structure:

$$t(\omega)=x(\omega)+iy(\omega)=\sqrt{T}e^{i\phi_t}, \tag{1}$$

where

$$\phi_t=\tan^{-1}(y/x)\pm m\pi$$

is the total phase accumulated as light propagates through the medium. The transmission $t(\omega)$ can be easily calculated using the well known matrix transfer method. ϕ_t contains all the information relating to the layered structure, such as refractive indices, number of layers, and layer thickness. The integer m is uniquely defined assuming $\phi_t(\omega)$ is a monotonically increasing function, and the condition that $m=0$ as $\omega\rightarrow 0$ is satisfied. This is important in order to calculate the proper phase of the field as a continuous function and to define the true effective index, as we will see below.

Beginning with the analogy of propagation in a homogeneous medium, we can express the total phase associated with the transmitted field as

$$\phi_t=k(\omega)D=\frac{\omega}{c}n_{\mathrm{eff}}(\omega)D, \tag{2}$$

where $k(\omega)$ is the effective wave vector and consequently n_{eff} is the effective refractive index that we attribute to the layered structure whose physical length is D.

The presence of gaps in the transmission spectrum, where the propagation of light is forbidden, suggests that the effective index of the structure should be complex. In particular, the index should have a large imaginary component inside the gap, to allow for nearly 100% scattering losses, i.e., reflections, and evanescent field modes. Thus we simply recast the transmission function as follows. First, we assume that $\sqrt{T}=|t|=e^{-\gamma D}$. This implies that an incident field of unit amplitude is ''attenuated'' by an amount $e^{-\gamma D}$, where $\gamma=(\omega/c)n_i$, and n_i is the imaginary component of the index. According to this picture, we write $\sqrt{T}=e^{\ln\sqrt{T}}$ and the complex transmission becomes $t=e^{\ln\sqrt{T}}e^{i\phi_t}=e^{i\phi}=x+iy$. Therefore,

$$i\phi=i\phi_t+\ln\sqrt{T}=i\left(\frac{\omega}{c}\hat{n}_{\mathrm{eff}}D\right), \tag{3}$$

where we still have $\phi_t=\tan^{-1}(y/x)\pm m\pi$, as before. Equation (3) then becomes:

$$\hat{n}_{\mathrm{eff}}(\omega)=(c/\omega D)[\phi_t-(i/2)\ln(x^2+y^2)]. \tag{4}$$

Equation (4) suggests that at resonance, where $T=x^2+y^2=1$, the imaginary part of the index is identically zero. Inside the gap, where the transmission is small, scattering losses are expected to be high, leading to evanescent waves.

We can also define the effective index as the ratio between the speed of light in vacuum and the effective phase velocity of the wave in the medium. We have

$$\hat{k}(\omega)=\frac{\omega}{c}\hat{n}_{\mathrm{eff}}(\omega). \tag{5}$$

Once the effective index has been defined, Eq. (5) represents the general dispersion relation of the layered structure, without any specific condition of periodicity. It is interesting to

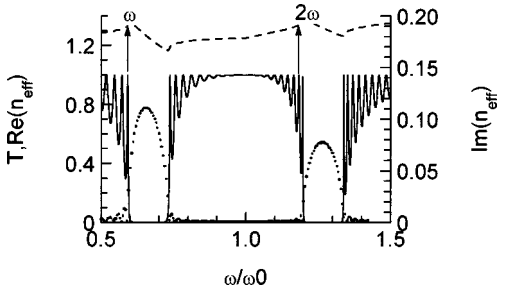

FIG. 1. Mixed quarter-wave/half-wave 1D PBG, $n_1=1$, $n_2=1.42857$, $N=20$ periods. Continuous line, transmission spectrum; dotted line, imaginary part of the effective index; dashed line, real part of the effective index. We note that for this layer configuration the first- and second-order gaps are separated by approximately a factor of 2. In contrast, in a quarter-wave stack the first- and second-order gaps are separated by a factor of 3.

note that from the dispersion equation we can also define a ''group index'' in terms of the real part of the effective index in the usual way:

$$n_g(\omega)=c\frac{dk}{d\omega}=n_{\mathrm{eff}}(\omega)+\omega\frac{dn_{\mathrm{eff}}(\omega)}{d\omega}. \tag{6}$$

Usually, the dispersion relation for periodic structures is obtained by applying periodic boundary conditions to the wave equation for an infinite, *periodic* structure. According to Bloch's theorem, Eq. (5) reduces to $\cos[k(\omega)d]=1/2\mathrm{Tr}[M]$, or

$$\cos[k(\omega)d]=\left[\cos\left(\frac{n_1\omega a}{c}\right)\cos\left(\frac{n_2\omega b}{c}\right)-\frac{n_1^2+n_2^2}{2n_1n_2}\sin\left(\frac{n_1\omega a}{c}\right)\sin\left(\frac{n_2\omega b}{c}\right)\right]. \tag{7}$$

Here, M is the scattering matrix for the elementary unit cell; n_1 and n_2 are the refractive indices of layers of thickness a and b respectively; $d=a+b$. Equation (7) is valid strictly for a periodic structure with an infinite number of layers. In contrast, our approach was developed principally for finite structures. We note, however, that our model is in complete agreement with the results of Eq. (7), provided the structure is periodic and the number of periods is large. The validity of Eqs. (4, 5) is general because it holds for any kind of layered structure, periodic or not.

As an example, let us consider the 20-period, quarter-wave/half-wave structure already discussed in Ref. [8] [see Fig. 1]. We construct the transmission function $t(\omega)$ and use the results to calculate the effective index, as given by Eq. (4). In Fig. 1 we plot the components of the effective index of refraction. We note that the real part of the index displays anomalous dispersion inside the gap. The imaginary component is small and oscillatory in the pass bands; it attains its maximum at the center of each gap, where the transmission is a minimum, and it is identically zero at each transmission resonance, as expected. We will have more to say on the similarities and differences between our effective wave vector and Bloch's vector in a separate publication. Suffice it to say here that the Kramers-Kronig relations for the effective

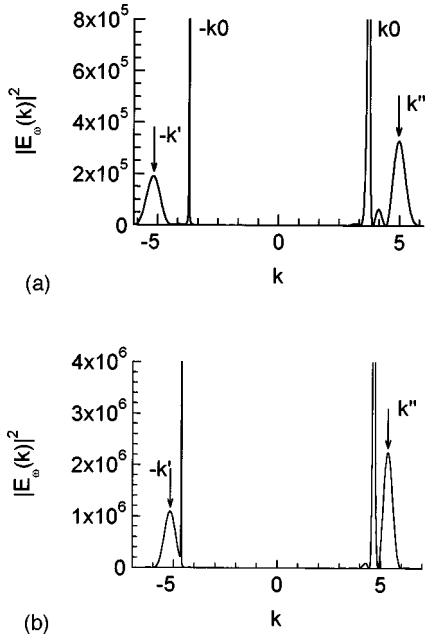

FIG. 2. Fourier components for pump wave packets at a time when the peak of the pulse reaches the structure of Fig. 1. (a) For pump tuned to a low-frequency band edge, $\omega/\omega_0=0.591$; $\pm k_0$ are free-space components associated with the part of the pulse located in the free space surrounding the structure; $-k'$ and k'' are the carrier wave vectors inside the structure, are transient, and correspond to the effective wave vectors. (b) Pump is tuned to the high-frequency band edge, $\omega/\omega_0=0.738$. Note that the relative location of the reflected peaks is shifted with respect to the forward-moving components, and with respect to the reflected components of (a) above. This comes as a result of anomalous dispersion across the photonic band gap.

index are identically satisfied, as we will see below. That is, given the imaginary part of the effective index as $\mathrm{Im}(n_{\mathrm{eff}})=(\frac{1}{2})\ln(x^2+y^2)$, the real part of the effective index is recovered.

The validity of the effective index can be demonstrated by direct numerical integration of Maxwell's equations. A pulse transmitted through a PBG structure ''sees'' an effective index given by the simple approach that we have presented above (an example is given in Fig. 2 for the same parameter of the layered structure of Fig. 1). In the calculation, we use a Gaussian input pulse that is approximately 1 ps in duration, tuned to the first resonance near the first-order band edge, at $\omega/\omega_0=0.591$ [see Fig. (1)]. Pulse length is hundreds of times longer compared to the length of the structure [8], pulse bandwidth is much smaller than band-edge transmission resonances so that most of the pulse is transmitted without scattering losses of distortions, *and the interaction is linear*. In Fig. 2(a), we plot the Fourier transform $|E_\omega(k)|^2$ of the incident pump field as a function of the wave vector k when the peak of the pulse has reached the structure. In the dynamics, four components can be identified. Two correspond to free-space propagation, at $\pm k_0$, i.e., portions of the pulse have been transmitted and reflected from the structure. The other two components are transient, and they are clearly visible as long as energy lingers inside the structure. An analysis of the other two components reveals that the locations of the ''center of gravity'' of the forward moving wave

packet k'' and the backward moving wave packet $-k'$ are consistent with the simple effective index calculations. At the same time, we note that the $-k'$ component is slightly shifted, indicating the existence of a different dispersion relation for forward and backward waves.

The wave packets of Fig. 2(a) are quite broad, and their widths correspond to a range of wave vectors. Unlike the free-space components at $\pm k_0$, the widths of the wave packets at $-k'$ and k'' are independent of incident pulse width, an effect that persists in the quasimonochromatic wave regime. We interpret this effect as a consequence of the sudden confinement of the incident wave to a space of width D, which excites a range of wave vectors such that $\delta k \cong 1/D$.

In Fig. 3, we depict the effective indices upon transmission for a 2-, a 10-, and a 20-period structure, and compare with the results of the dispersion relation for infinite structure. This figure makes it clear that the effective, dispersive properties of the structures are modified by the number of periods, and converge to the infinite-structure results increasing the number periods.

It can be shown numerically that the real and imaginary parts of the complex effective index identically satisfy the Kramers-Kronig (KK) relations. Starting with the imaginary part of the effective index $n_I(\omega)$, [see Fig. 1(a)] which is proportional to $\ln\sqrt{T}$, we apply the usual KK relations and obtain the real part of the effective index as follows:

$$n_R(\omega) - n_R(\infty) = \frac{2}{\pi} P \int_0^\infty \frac{\omega' n_I(\omega') d\omega'}{(\omega')^2 - \omega^2}, \tag{8}$$

where $n_R(\infty) \approx (\Sigma_{i=1}^N n_i d_i)/(\Sigma_{i=1}^N d_i)$, where n_i and d_i are the refractive index and the thickness of the ith layer, respectively. We note that the effective index has asymptotic behavior at high frequencies. Therefore, beginning with the knowledge of the imaginary part, i.e., the modulus of the transmission, it is possible to recover the real part of the index for any kind of layered structure by simple application of Eq. (8). This equation explicitly shows that the transmission coefficient $t(\omega)$ is a causal function, i.e., its Fourier transform is identically zero for negative times [19], and intrinsically implies the monotonic growth of the phase as a function of frequency. These results lend further credence to the validity of the effective index approach.

III. PHASE MATCHING THROUGH EFFECTIVE INDEX FOR A FINITE PERIODIC STRUCTURE

The effective index approach that we have developed in the preceding sections allows us to define and evaluate phase-matching conditions for parametric interactions in any kind of layered structure in a simple way. We emphasize that up to this point we have made use of the linear properties of the structures. In a second-harmonic generation process, imposing phase-matching conditions is equivalent to imposing the condition of equal phase velocities for the fields propagating inside the structure. That is, we require [17]

$$\hat{n}_{\text{eff}}(\omega_1) = \hat{n}_{\text{eff}}(\omega_2). \tag{9}$$

For a *finite, N-period* structure, the real part of the effective index can also be expressed in terms of the geometrical parameters of a structure with an infinite number of periods, the Bloch phase in particular [20], defined as $\beta = K_\beta \Lambda$. Here, K_β is the Bloch vector defined in Eq. (7) above, where $k(\omega) \equiv K_\beta$ and $\Lambda = a + b$ is the length of the unit cell. The results in Ref. [8] suggest that the nonlinear interaction is maximized at the resonances near the band edge. We would like to test the predictions of the effective index model regarding the existing phase-matching conditions and compare with the results of Ref. [8]. We tune the pump at a resonance peak where the transmission is unity and the imaginary part is zero. According to the results in Ref. [20], we can write an explicit analytic expression for the real part of the effective index. That is, Eq. (4) becomes

$$n_{\text{eff}} = \frac{1}{\alpha}\tan^{-1}[y/x] \pm \frac{m\pi}{\alpha} = \frac{1}{\alpha}\left\{ \pm \pi m + \tan^{-1}\left[\frac{y_1 \sin N\beta}{x_1 \sin N\beta - (x_1^2 + y_1^2)\sin(N-1)\beta} \right] \right\}. \tag{10}$$

y_1 and x_1 are the imaginary and real parts of the transmission of the elementary cell of the structure, which is repeated N times, $\alpha = (\omega/c)D$. m is an integer number that is not arbitrary; it is a function of frequency, due to the fact that the phase shift in transmission between consecutive resonances is π. It can be obtained following the assumption that $m = 0$ at $\omega = 0$, as before, and $\phi_t(\omega)$ is a monotonically increasing function. It is also possible to express m as a function of the Bloch phase: if we consider that the transmission $T(\beta)$ is a periodic function of period π/N, and two consecutive resonances correspond to $\Delta\beta = \pi/N$ and $\Delta m = 1$, then

$$m = \text{int}\left[\frac{N\beta}{\pi} + \frac{1}{2} \right]. \tag{11}$$

Here int is the integer part, with a range of definition of the tangent function between $-\pi/2$ and $+\pi/2$. Therefore, the phase of the transmitted field in terms of the Bloch phase is

$$\phi_t = \tan^{-1}[z \tan(N\beta)\cot g(\beta)] + \text{int}\left[\frac{N\beta}{\pi} + \frac{1}{2} \right]\pi, \tag{12}$$

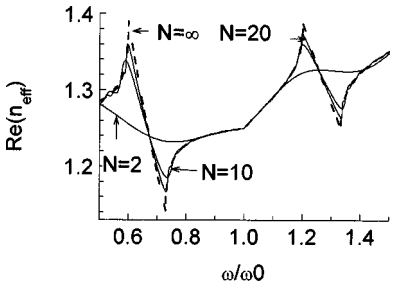

FIG. 3. Same refractive indices as Fig. 1, but with $N = 2,10,20$, and an infinite number N of periods, as indicated by the arrows. Note the dependence on N of the dispersion around the band edges. There is a noticeable kink around $\omega/\omega_0 = 1$ due to the sudden onset of dispersion, which is necessary in this case to tune the resonances as depicted in Fig. 1.

where $z=y_1/x_1$. Equation (10) essentially states that knowledge of the properties of the unit cell, the number of periods, and the Bloch phase completely determines the effective index of the N-period, finite structure. Equation (12) contains additional information regarding the location of the resonances where phase-matching conditions for second-harmonic generation can be realized. Locating the fundamental field at the first resonance near the band edge, we have

$$\beta_1=\frac{\pi}{N}(N-1). \tag{13}$$

Substituting Eq. (13) into Eq. (12), we obtain an expression for the phase of the fundamental field:

$$\phi_1=\mathrm{int}\left[\frac{N\beta}{\pi}+\frac{1}{2}\right]=\pi(N-1). \tag{14}$$

Now, imposing the phase-matching condition for the second-harmonic generation process, namely, $2K_1(\omega_1)=K(\omega_2)$, we obtain

$$n_1(\omega_1)=\frac{\phi_1}{\alpha}=n_2(\omega_2)=\frac{\phi_2}{2\alpha}, \tag{15}$$

which leads to

$$\pi(N-1)=\tfrac{1}{2}\tan^{-1}[z_2\tan(N\beta_2)\cot g(\beta_2)]+\mathrm{int}\left[\frac{N\beta_2}{\pi}+\frac{1}{2}\right]\frac{\pi}{2}, \tag{16}$$

where the subscript 2 refers to the second-harmonic field. We denote the value of the integer part of the second term on the right-hand side of Eq. (16) as M. Consequently, we have

$$\tan^{-1}[z_2\tan(N\beta_2)\cot g(\beta_2)]=\pi(2N-2-M). \tag{17}$$

As before, the range of the inverse tangent function is satisfied when $M-2N+2=0$. Therefore,

$$\beta_2=\frac{\pi}{N}(2N-2). \tag{18}$$

Taken together, Eqs. (13) and (18) state that the pump field should be tuned to the $N-1$ transmission resonance, which corresponds to the first resonance near the first-order band edge, and the second harmonic field should be tuned to the $2N-2$ resonance, which corresponds to the second resonance away from the second-order band edge for the mixed half-wave/quarter-wave structure. This phase-matching condition that we find using the effective-index approach is identical to the results reported in Ref. [8], where a systematic study was undertaken using short pulses in order to find the optimal conversion efficiency. From Eqs. (13) and (18), we thus arrive at the following simple, phase-matching condition:

$$\beta_2(2\omega)=2\beta_1(\omega). \tag{19}$$

Equation (19) is not a totally unexpected result. According to the formalism we have developed above, the effective-index approach takes into account effects due to the finite size of the structure. More importantly, the approach includes the influence of all the interfaces that make up the structure, including input and output interfaces, regardless of their geometrical disposition. In this way, we can predict that for the optimal, phase-matched SHG process in a finite, periodic structure, the pump field should be tuned to the low-frequency band edge, where the density of modes is a maximum, and the second harmonic field should be tuned to the second-transmission resonance near the second-order band edge [8], precisely as Eqs. (13), (18), and (19) suggest.

In general, we also predict similar behavior at the high-frequency band edge, and expect that this approach can be applied to any problem where some kind of phase-matching condition is required for efficient nonlinear frequency conversion, including third-harmonic generation, and in the more general case of parametric up- and down-conversion, which we are currently studying.

To conclude this section, we note that Fig. 1 also depicts the real part of the effective index of refraction, and we note that the effective-index model accurately predicts that phase-matching conditions are satisfied exactly as predicted by direct integration of the nonlinear propagation equations in the layered structure [8].

IV. EXAMPLES OF PHASE MATCHING CALCULATION IN THE PRESENCE OF MATERIAL DISPERSION

As discussed in Ref. [8], under phase-matching conditions the enhancement of second-harmonic generation in PBG's is attributed to the high density of modes near the band edges. As we saw above, the combination of high density of modes and exact phase-matching conditions can be achieved in a mixed half-quarter wave periodic PBG in such a way that the density of modes is high at both the fundamental and second-harmonic frequencies. Therefore, the geometry can be used to tune the fields with respect to the band edge, as in Fig. 1. If considerable material dispersion is present, phase-matching conditions can easily be spoiled and conversion efficiencies will be low even if the density of modes is high [8]. Nevertheless, one can still achieve phase matching by manipulating the geometry of the structure, in particular, layer thicknesses, angle of incidence, number of periods, and symmetry properties.

By way of example, we consider a periodic structure composed of AlN/SiO_2. We consider a range of wavelengths to have SHG in the blue spectral region, i.e., we tune the fundamental field at $\lambda_1=0.794\,\mu$m; the SH field is tuned at $\lambda_2=0.397\,\mu$m. The dispersive properties of AlN are described in Ref. [21]. In the selected wavelength range we may neglect absorption. SiO_2 also exhibits dispersion, which is also taken into account. Phase-matching conditions for second-harmonic generation for a mixed half-quarter stack can then be obtained by choosing a suitable reference wavelength, in this case is $\lambda_0=0.48\,\mu$m, and a suitable number of periods: $N=14$. The fundamental field (FF) is tuned at the first resonance near the band edge, and the SH field is tuned at the second resonance near the second-order band edge, in a manner similar to the depiction in Fig. 1; Fig. 4 shows part of the spectrum, i.e., the respective transmission resonance peaks for FF and SH as a function of the normalized fre-

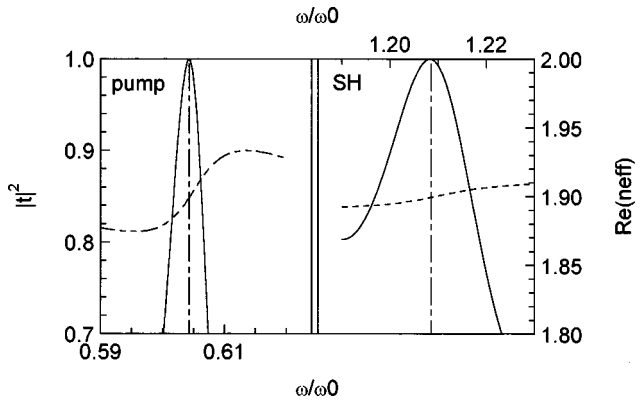

FIG. 4. Effective index (dotted line) superimposed on the transmission resonances (continuous line) at ω and 2ω, for $N=14$ periods of AlN/SiO_2 layers. FF at $\lambda_1=0.79\,\mu$m, and SH at $\lambda_2=0.397\,\mu$m.

quency ω/ω_0; Fig. 4 also shows the real part of the effective index (dotted curve) and shows that the phase-matching requirements imposed by Eq. (9) are satisfied. We note that calculation of the density of modes can also easily be accomplished using the matrix transfer method [20].

Up to now we have considered periodic structures. If material dispersion is strong, departures from periodicity may help achieve both phase-matching conditions and the necessary high density of states near the band edge. For example, adding one layer to a periodic structure will make it symmetric. Phase matching will then occur under a new set of parameters, which can be summarized as follows: $\lambda_0=0.445\,\mu$m; the FF wavelength is tuned to $\lambda_1=0.731\,\mu$m; and the SH is tuned to $\lambda_2=0.3655\,\mu$m.

As a final example, we briefly consider a 35-period stack composed of GaAs and AlAs layers. In order to have a nonzero nonlinear quadratic coefficient, it is necessary to use a suitable orientation of the GaAs crystal. This restricts the input angle for the pump field [22] (we have considered an incidence angle $\theta_0=48°$). In this case it is difficult, but not impossible, to compensate material dispersion with the geometrical dispersion introduced by layer arrangement. Building the stack beginning with GaAs/AlAs and ending with a GaAs layer to make it symmetric leads to good phase-matching conditions and high density of modes as before, provided the pump is tuned near 3 μm and the SH is tuned near 1.5 μm. In this case, the fundamental and second-harmonic fields are once again tuned as in Fig. 1, near their respective band edges. Figure 5(a) shows a range of values for the density of modes for first (continuous curve) and second harmonic (dotted curve) field, and for transverse electric (TE) polarization as a function of the wavelength. The vertical bar represents the location of the wavelengths for which phase-matching conditions are satisfied. We note that phase-matching conditions are not exact, but reasonably good. On the other hand, we find exact phase-matching conditions for transverse magnetic (TM) polarization [Fig. 5(b)] provided we use 27 periods plus one layer, and an input angle of 51°. Figure 5(b) also shows the density of modes versus wavelength for FF (continuous curve) and SH (dotted curve). As before, the vertical bars represent the wavelengths for which phase-matching conditions are satisfied.

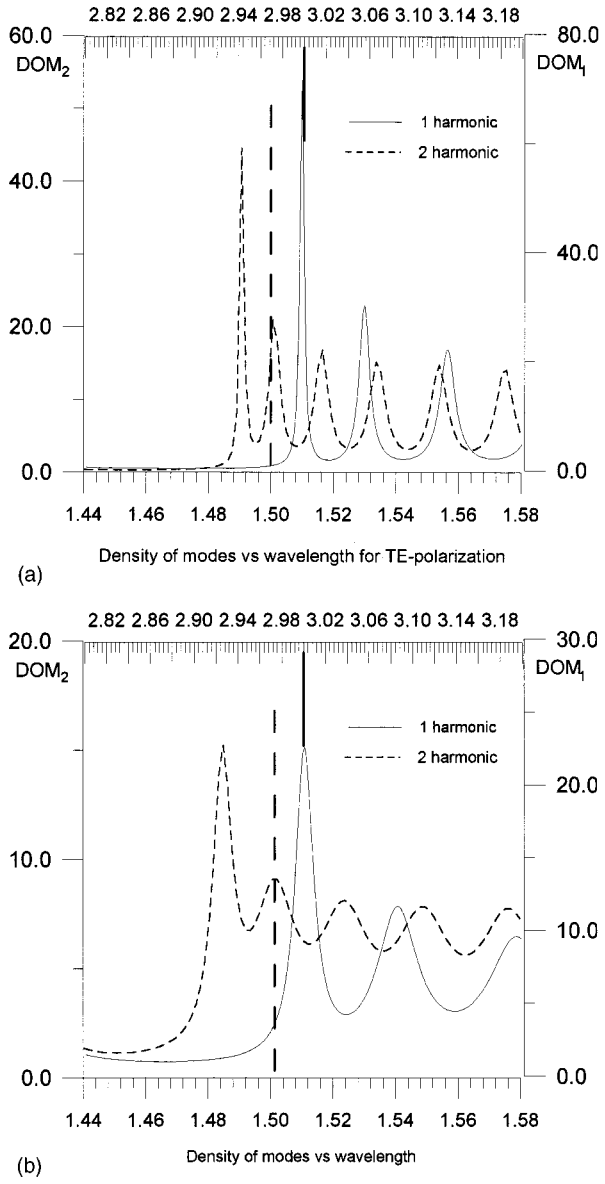

FIG. 5. Mixed quarter-wave/half-wave PBG structure composed of GaAs/AlAs. FF at $\lambda=3$ μm and SH at 1.5 μm. (a) Spectral density of modes for $N=35$ periods+1 layer of high refractive index, TE polarization, input angle of 48°. (b) Same as (a), with $N=27$ periods+1 layer of high refractive index, TM polarization, input angle of 51°.

V. PHASE OF THE FIELD UPON REFLECTION

In this section we analyze finite-size effects on the reflective properties of the structure near the band edge. We begin with the dispersion relation $k(\omega)=(\omega/c)n_{\text{eff}}(\omega)$. We can calculate the effective dispersion relation for reflected waves according the matrix transfer formalism, as we did for transmitted waves. For the reflected spectrum we can write

$$r=\sqrt{R}e^{i\phi_r}=r_x+ir_y. \tag{20}$$

We note that the phase accumulated by the reflected wave traveling from left to right (LTR) through the structure can be written as

$$\phi_r=\tan^{-1}(r_y/r_x)\pm m\pi. \tag{21}$$

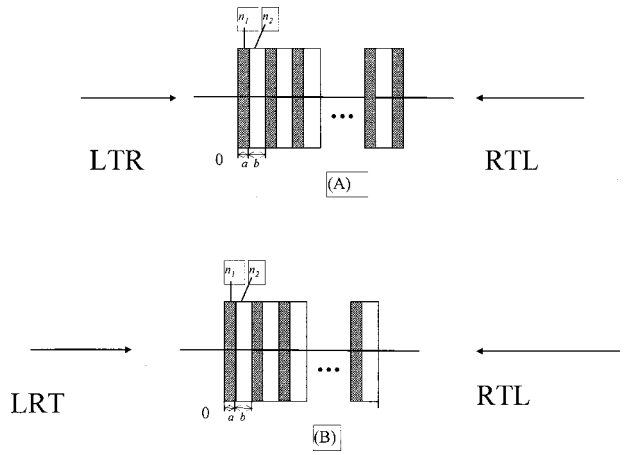

FIG. 6. Schematic representation of the waves traveling from left to right (LTR) and right to left (RTL) for symmetrical (A) and periodic (B) geometry.

The reflected effective index can be obtained as follows:

$$\phi_r = k_0 \hat{n}_{\text{eff}}(r) D, \tag{22}$$

where $n_{\text{eff}}(r)$ is the real part of the reflected effective index seen by the LTR reflected wave (see Fig. 6). More care must be exercised when calculating the dispersion relation for the reflected fields. Using symmetry considerations between LTR and RTL (right to left) incident waves, it can be shown that [23,24] $r^-(\omega) = -\{r^+(\omega)\}^*[t(\omega)/t^*(\omega)]$, where $\pm$ refers to LTR and RTL, respectively. Defining LTR and RTL reflection coefficients in a manner similar to the definition of the transmission coefficient in Sec. II, namely, $r^{\pm} = |r| e^{i\phi_r^{\pm}}$, it follows that

$$\tilde{\phi}(\omega) = \frac{\phi_r^+(\omega) + \phi_r^-(\omega)}{2} = \phi_t(\omega) \pm \frac{\pi}{2} j, \quad j = 1,3,5 \ldots . \tag{23}$$

Equation (23) suggests that LTR and RTL phases cannot be related unambiguously, and the solution to Eq. (23) is not unique. Alternatively, Eq. (23) allows us to define upper and lower bounds for the average reflected phase. Suffice it to say here that, in general, RTL and LTR propagation cannot be considered separately, and that ambiguities can be removed by solving Maxwell's equations in the time domain, as we do here. In general, the phase and amplitude of the transmission coefficient are the same for LTR and RTL propagating waves; the related effective indices will also be indistinguishable for RTL and LTR propagation. This is generally not true for reflected waves. The ambiguity can be extended to the effective index directly from Eq. (23):

$$n_{\text{eff}}(r) = n_{\text{eff}}(t) \pm \frac{\pi}{2 k_0 D} j, \quad j = 1,3,5, \tag{24}$$

where (t) and (r) refer to the transmitted and reflected fields, respectively. Because of the sign ambiguity, we find that it is not possible to verify the Kramers-Kronig relations for the reflected effective complex index.

Equation (24) suggests that the ambiguity can only be eliminated in the case of structures of infinite length. We show the convergence properties of the effective indices in Figs. 7, where we plot the index calculated from the average phase in Eq. (22) for 20 [Fig. 7(a)] and 200 periods [Fig. 7(b)]. In the limit of large number of periods, there is virtually no difference between RTL and LTR propagation variables, regardless of the symmetry properties of the structure.

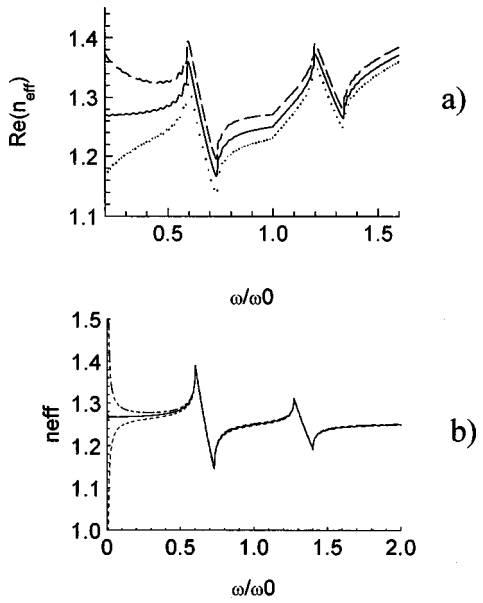

FIG. 7. Example of reflected upper (dotted) and lower (dashed) boundary values, and transmitted (solid) effective index, for the structure of mixed quarter-wave/half-wave structure, $n_1 = 1$, $n_2 = 1.42857$, for (a) 20 periods, and (b) 200 periods.

The evidence that indeed forward and backward effective indices are different can once again be found in the direct integration of Maxwell equations in the time domain. An example is given in Fig. 2. The pulse is tuned at the first resonance near the low-frequency band edge (see Fig. 1), and we plot the Fourier transform of the field. As we mentioned in Sec. II, the center of gravity of the wave packets corresponding to transient components k' and k'' leads us to conclude that forward and backward components indeed propagate with different phase velocities. We find that the results obtained by direct integration of the equations of motion generally agree with the effective index calculation, and we conclude that these results come about as a direct consequence of truncating the structure, and breaking the translational invariance of the system. This point is further emphasized in Fig. 2(b). This figure is a pictorial representation of the Fourier components of an input pulse as in Fig. 2(a), but tuned to the first transmission resonance near the high-frequency band edge. Comparison of Figs. 2(a) and 2(b) clearly shows that the relative location of the center of gravity of the backward-propagating wave vector changes with respect to the freely propagating components. That is, in Figs. 2(a) and 2(b), the magnitude of the location of the center of gravity of the reflected wave packet at $-k'$ is larger at the low-frequency band edge. This behavior is unexpected, but is consistent with the results of the simpler effective index model, which predicts anomalous dispersion across the photonic band gap, and discrepancies between forward and backward wave vectors in the case of finite structures.

VI. CONCLUSIONS

We have presented results relating to the effects of boundary conditions on the dispersive properties of finite multilayered stacks. In particular, we have developed an effective index approach specifically for one-dimensional finite structures, and have highlighted the concept for the study of phase-matching conditions in parametric nonlinear interactions in photonic band-gap materials, although we focused our attention on second-harmonic generation processes.

The effective-index approach takes into account the dispersion introduced by the geometry of the materials we are considering, including input and output interfaces. The number of interfaces, and the presence of input and output boundaries, causes fundamental modifications in the phase velocity of backward and forward components of the field in a way which is strictly connected to the specific geometry under consideration. The influence of the input and output interfaces is strongly felt near the band edges, and we have shown that these effects disappear for structures of infinite length. Our results can only inspire caution when results obtained for structures of infinite length are generalized to structures of finite length, especially without the benefit of a simple verification of propagation effects in real, finite systems. We have also shown that using the effective index approach phase matching conditions can be found for almost any kind of layered structure.

To summarize, the effective index approach provides a unique, simple, and fast method to achieve and optimize phase matching conditions in dispersive media via the matrix transfer method. Normal material dispersion can be overcome by proper choice of layer thicknesses, angle of incidence, number of periods, and symmetry properties.

PBG structures offer several other advantages, such as increased density of modes, large field enhancements, low group velocity, and field overlap for the enhanced conversion efficiency relative to phase-matched bulk crystals. These results are valid for layered structures with large index contrast, long grating structures, waveguides having small index modulation depth, and structures that are not periodic.

Finally, the analogy that is usually drawn between photonic and electronic band structure brings us full circle to predict the same phenomena described above for electrons in finite, solid-state nanostructures. While we cannot predict with certainty what effects can be expected for electron waves in matter, the concept is very intriguing and merits further investigation.

[1] E. Yablonovitch, Phys. Rev. Lett. **58**, 2059 (1987).

[2] J. D. Joannopoulos and P. R. Villeneuve, Nature (London) **386**, 143 (1997).

[3] C. M. Soukoulis, Phys. Scr. **T66**, 146 (1996).

[4] M. Scalora, J. P. Dowling, C. M. Bowden, and M. J. Bloemer, Phys. Rev. Lett. **73**, 1368 (1994).

[5] M. Scalora, J. P. Dowling, M. J. Bloemer, and C. M. Bowden, J. Appl. Phys. **76**, 2023 (1994).

[6] J. P. Dowling, M. Scalora, M. J. Bloemer, and C. M. Bowden, J. Appl. Phys. **75**, 1896 (1994).

[7] M. Scalora, R. J. Flynn, S. B. Reinhardt, R. L. Fork, M. D. Tocci, M. J. Bloemer, C. M. Bowden, H. S. Ledbetter, J. M. Bendickson, J. P. Dowling, and R. P. Leavitt, Phys. Rev. E **54**, R1078 (1996).

[8] M. Scalora, M. J. Bloemer, A. S. Manka, J. P. Dowling, C. M. Bowden, R. Viswanathan, and J. W. Haus, Phys. Rev. A **56**, 3166 (1997).

[9] M. Scalora, M. J. Bloemer, A. S. Pethel, J. P. Dowling, C. M. Bowden, and A. S. Manka, J. Appl. Opt. **83**, 2377 (1998).

[10] J. C. Knight, T. A. Birkes, P. Russel, J. P. De Sandro, J. Opt. Soc. Am. A **15**, 748 (1998).

[11] E. Yablonovich, Microwave J. **VI**, 66 (1999).

[12] N. Bloembergen and A. J. Sievers, Appl. Phys. Lett. **17**, 483 (1970).

[13] M. J. Steel and C. M. de Sterke, Appl. Opt. **35**, 3211 (1996).

[14] J. Martorell and R. Corbalan, Opt. Commun. **108**, 319 (1994).

[15] J. Trull, R. Vilaseca, J. Martorell, and R. Corbalan, Opt. Lett. **20**, 1746 (1995); J. Martorell, R. Vilaseca, and R. Corbalan, Appl. Phys. Lett. **70**, 702 (1997).

[16] D. J. Lovering, G. Fino, C. Simonneau, R. Kuszelewicz, R. Azoulay, and J. A. Levenson, Electron. Lett. **32**, 1782 (1997).

[17] A. Jariv and P. Yen, J. Opt. Soc. Am. **67**, 438 (1977).

[18] J. P. Dowling and C. Bowden, J. Mod. Opt. **41**, 345 (1994).

[19] J. Pankove, *Optical Processes in Semiconductors* (Dover, NY, 1975).

[20] J. M. Bendickson, J. P. Dowling, and M. Scalora, Phys. Rev. E **53**, 4107 (1996).

[21] D. Brunner, H. Angere, E. Bustarret, F. Freudenberg, R. Hopler, R. Dimitrov, O. Ambacher, and M. Stutzmann, J. Appl. Phys. **82**, 5090 (1997).

[22] C. Simonneau, J. P. Debray, J. C. Harmad, P. Violokavic, D. J. Lovering, and J.A. Levenson, Opt. Lett. **22**, 1175 (1997).

[23] L. Poladian, Opt. Lett. **22**, 1571 (1997).

[24] J. P. Dowling, IEE Proc.-J: Optoelectron. **145**, 420 (1998), special issue on photonic crystals and photonic microstructures.